Adaptive Robust Optimization for Operation of Active Distribution Networks in Real-time Energy Markets

Ali Arab-Kuhsar, Morteza Rahimiyan, *Senior Member, IEEE*, Pierluigi Siano, *Senior Member, IEEE*, and Mahsa Azarnia, *Student Member, IEEE*

***Abstract*—Energy management system (EMS) and volt-var optimization (VVO) programs are jointly employed to achieve the efficient operation of active distribution networks (ADNs). However, current studies often overlook that the operation of ADNs is coupled with trading energy in real-time (RT) energy markets. To fill this gap, this paper develops an adaptive robust optimization (ARO) model of ADNs in RT energy markets. The studied ADN consists of photovoltaic (PV) units, electric vehicle (EV) charging stations, and flexible demands interconnected through a medium-voltage distribution network. Through the proposed model, the integrated EMS and VVO programs can decide to offer energy in the hourly RT energy market, schedule flexible demands, and adjust slow-acting devices (e. g., on-load tap changers and capacitors), while anticipating the operation conditions of the ADN under uncertain prices, charging power level of EVs, and available PV power generation through the uncertainty sets. Once the market outcomes are known, the integrated EMS and VVO programs dispatch the fast-acting devices of PV units and EV charging stations. The results of a realistic case study indicate that prioritizing the reduction of voltage violations leads to lower energy trading in the RT energy market and a decrease in profit.**

***Index Terms*—Active distribution network (ADN), energy management system (EMS), volt-var optimization (VVO), energy market, electric vehicle (EV) charging station, adaptive robust optimization.**

NOMENCLATURE

A. Sets and Indices

Ω_b^{C}	Set of capacitors connected to bus b
Ω_b^{D}	Set of demands on bus b
Ω^{L}	Set of lines
Ω^{MG}	Set of buses connected to main grid
Ω_b^{O}	Set of on-load tap changers (OLTCs) connected to bus b
Ω_b^{PV}	Set of photovoltaic (PV) units connected to bus b
Ω_b^{S}	Set of electric vehicle (EV) charging stations connected to bus b
Φ^{X}	Set including first-stage continous and binary decision variables
Φ^{Y}	Set including second-stage decision variables
b, Ω^{B}	Index and set of buses
c, Ω^{C}	Index and set of capacitors
d, Ω^{D}	Index and set of demands
g, Ω^{PV}	Index and set of PV units
h	Index of column-and-constraint generation (CCG) repetition
o, Ω^{O}	Index and set of OLTCs
p, $\Omega_o^{\mathrm{O,T}}$	Index and set of tap positions of OLTC o
s, Ω^{S}	Index and set of EV charging stations
t, Ω_τ^T	Index and set of time periods in hourly scheduling horizon $[\tau, T]$

B. Parameters

$\alpha_{d,t}^{\mathrm{P}}$, $\beta_{d,t}^{\mathrm{P}}$	Constant power components of impedance-power (ZP) load model for demand d at time t
$\alpha_{d,t}^{\mathrm{Z}}$, $\beta_{d,t}^{\mathrm{Z}}$	Constant impedance components of ZP load model for demand d at time t
Δ_t	Power-energy conversion factor
$\eta_s^{\mathrm{ST,C}}$, $\eta_s^{\mathrm{ST,D}}$	Charging and discharging efficiencies of energy storage system (ESS) located at EV charging station s
$\Gamma_s^{\mathrm{EV,C}}$	Uncertainty budget related to charging power level of EVs located at EV charging station s

Manuscript received: May 27, 2025; revised: August 21, 2025; accepted: January 9, 2026. Date of CrossCheck: January 9, 2026. Date of online publication: February 12, 2026.

A. Arab-Kuhsar, M. Rahimiyan, and M. Azarnia are with Energy Systems Planning and Operation (ESPO) Lab., Faculty of Electrical Engineering, Shahrood University of Technology, Shahrood, Iran (e-mail: Ali_Kuhsar1996@yahoo.com; Morteza.Rahimiyan@shahroodut.ac.ir; Mahsa.Azarnia@yahoo.com).

P. Siano (corresponding author) is with Department of Management & Innovation Systems, University of Salerno, Salerno, Italy, and he is also with the Department of Electrical and Electronic Engineering Science, University of Johannesburg, Johannesburg 2006, South Africa (e-mail: PSiano@unisa.it).

DOI: 10.35833/MPCE.2025.000481

Γ^{PV}, Γ^{RT} Uncertainty budgets related to PV power generation and real-time (RT) energy market price

λ_t^{RT} RT energy market price at time t

ω Penalty factor of voltage violations

$\overline{E}_s^{\mathrm{ST}}$, $\underline{E}_s^{\mathrm{ST}}$ The maximum and minimum energy limits of ESS located at EV charging station s

$\bar{I}_{bl}$ The maximum admissible current through line (b,l)

$\overline{P}_{d,t}^{\mathrm{D}}$, $\underline{P}_{d,t}^{\mathrm{D}}$ The maximum and minimum active power levels of demand d at time t

$\overline{P}_{s,t}^{\mathrm{EV,C}}$ Charging level of active power of EVs at EV charging station s at time t

$\overline{P}^{\mathrm{M}}$ The maximum active power that can be traded with RT energy market

$\overline{P}_{g,t}^{\mathrm{PV}}$ Available active power generation of PV unit g at time t

$\overline{P}_{s,t}^{\mathrm{PV,S}}$ Available active power generation of PV unit located at EV charging station s

$\overline{P}_s^{\mathrm{ST,C}}$, $\overline{P}_s^{\mathrm{ST,D}}$ The maximum charging and discharging levels of active power of ESS located at EV charging station s

PF_d^{D} Power factor for demand d

$\underline{PF}_g^{\mathrm{PV}}$ The minimum power factor of PV unit g

$\overline{Q}_c^{\mathrm{CAP}}$ Reactive power capacity of capacitor c

$\overline{Q}_s^{\mathrm{S}}$, $\underline{Q}_s^{\mathrm{S}}$ The maximum and minimum reactive power levels of EV charging station s

R_{bl}, X_{bl} Resistance and reactance of line (b,l)

$R_d^{\mathrm{D,U}}$, $R_d^{\mathrm{D,D}}$ Demand pick-up and drop ramping limits for demand d

$\overline{S}_g^{\mathrm{PV}}$ Apparent power capacity of PV unit g

$\overline{S}_b^{\mathrm{MG}}$ Apparent power capacity of main grid connection at bus b

$\overline{S}_s^{\mathrm{S}}$ Apparent power capacity of EV charging station s

T Length of scheduling horizon

$U_{d,t}^{\mathrm{D}}$ Utility function of energy consumption by demand d at time t

$U_{s,t}^{\mathrm{EV,C}}$ Price of energy consumption by EVs at EV charging station s at time t

$\overline{V}_b$, $\underline{V}_b$ The maximum and minimum admissible limits of voltage at bus b

$V_{0,t}$ Voltage of main grid

$X_{o,p}^{\mathrm{O,T}}$ Square of tap ratio of OLTC o in position p

C. Variables

$\overline{\Delta v}_{b,t}$, $\underline{\Delta v}_{b,t}$ Voltage violations from the maximum and minimum admissible values at bus b at time t

ϵ Total voltage violation

$e_{s,t}^{\mathrm{ST}}$ Energy stored in ESS located at EV charging station s at time t

$i_{bl,t}$, $l_{bl,t}$ Current and squared current flows through line (b,l)

$p_{d,t}^{\mathrm{D}}$, $q_{d,t}^{\mathrm{D}}$ Active and reactive power levels of demand d at time t

$p_{d,t}^{\mathrm{D,S}}$, $q_{d,t}^{\mathrm{D,S}}$ Scheduled active and reactive power levels of demand d at time t

$p_{bl,t}^{\mathrm{L}}$, $q_{bl,t}^{\mathrm{L}}$ Active and reactive power flows through line (b,l) at time t

p_t^{M} Active power traded in RT energy market at time t

$p_{b,t}^{\mathrm{MG}}$, $q_{b,t}^{\mathrm{MG}}$ Active and reactive power injected from main grid to bus b at time t

$p_{g,t}^{\mathrm{PV}}$, $q_{g,t}^{\mathrm{PV}}$ Active and reactive power generated by PV unit g at time t

$p_{s,t}^{\mathrm{PV,S}}$ Active power generated by PV unit located at EV charging station s at time t

$p_{s,t}^{\mathrm{S}}$, $q_{s,t}^{\mathrm{S}}$ Active and reactive power injections by EV charging station s at time t

$p_{s,t}^{\mathrm{ST,C}}$, $p_{s,t}^{\mathrm{ST,D}}$ Charging and discharging levels of active power of ESS located at EV charging station s at time t

$q_{c,t}^{\mathrm{CAP}}$ Reactive power injection by capacitor c at time t

$r_{o,p,t}^{\mathrm{O,T}}$ Binary variable showing status of tap position p of OLTC o at time t

$s_{c,t}^{\mathrm{CAP}}$ Binary variable indicates status of capacitor c at time t

$v_{b,t}$, $u_{b,t}$ Voltage and squared voltage at bus b at time t

I. INTRODUCTION

THE operation of distribution networks has become increasingly complex due to the rising penetration of conventional and stochastic renewable power generation, electric vehicles (EVs), and flexible demand resources, all of which exhibit diverse techno-economic characteristics and inherent variability [1]. Recent advancements in smart grid technologies have enabled system operators to coordinate these assets more effectively, transforming traditional distribution networks into active distribution networks (ADNs) with enhanced operational flexibility. Leveraging these capabilities, ADNs can actively participate in energy markets as both buyers and sellers [2], whereas conventional distribution networks typically operate solely as market buyers.

The energy management system (EMS) of an ADN can strategically participate in both the day-ahead [3] and hour-ahead real-time (RT) energy markets [4], making informed scheduling decisions for energy transactions and asset coordination ahead of power delivery. However, fluctuations in market prices and deviations from scheduled energy delivery introduce both technical and financial risks to the energy management of an ADN. To mitigate these risks, the EMS can exploit the operational flexibility of conventional generation units, demand-side resources, and energy storage systems (ESSs).

The mutual dependency between decisions made by the EMS and other operational applications is unavoidable, posing significant challenges to the operation of ADNs. On one hand, energy schedules determined by the EMS affect voltage profiles across the distribution network, which are regulated by volt-var optimization (VVO) to maintain voltages within admissible limits close to RT operation [5]. This interaction arises from the inherent coupling between active and reactive power flows in distribution systems, particularly in low-voltage feeders with high resistance-to-reactance (*R*/*X*) ratios, where variations in active power injections or withdrawals can lead to pronounced voltage deviations. To address these deviations, VVO coordinates both slow-acting devices such as on-load tap changers (OLTCs) and capacitor banks, which are typically adjusted on an hourly basis [5], and fast-acting devices such as inverter-based photovoltaic (PV) units and ESSs, which are capable of providing reactive power support over shorter timeframes (e. g., minutes) [6]. On the other hand, due to the behavior of voltage-dependent load, voltage adjustments implemented by the VVO can alter real power losses, reactive power flows, and end-use consumption, thereby leading to deviations from the energy schedules established by the EMS [7]. These nonlinear and time-varying interactions hinder the decoupling of EMS and VVO objectives, increasing coordination complexity and potentially creating conflicts between economic efficiency and technical feasibility. Consequently, effective coordination between EMS-based energy scheduling and VVO-controlled device settings is essential to ensure efficient and reliable operation of ADN.

Most existing studies [6], [8]-[22] on the integrated EMS and VVO of ADNs primarily address the techno-economic characteristics of electrical assets such as distributed generation, ESSs, loads, and EVs, as well as power flow modeling in distribution networks including approximation and relaxation techniques. However, several critical challenges remain open and require further investigation: ① the operation of EV charging stations [8]-[11]; ② uncertainty sources and their handling approaches [6], [8]-[22]; and ③ participation in energy markets [21], [22]. To provide deeper insight, relevant studies are reviewed according to these categorized challenges as follows.

The high penetration of EVs can push the distribution network beyond its admissible operational limits, making it essential to optimally schedule the EV charging stations to prevent overloading and voltage violations. To address this issue, a step-by-step methodology is proposed in [8] to minimize the operational costs by scheduling EV charging during low-price intervals and curtailing energy consumption when full charging cannot be achieved. With VVO enabled, the minimum voltage profile is maintained close to the lower boundary. In [9], a central supervisory and resilient distributed control strategy for fast EV charging stations is proposed to ensure compliance with grid codes for active and reactive power flows. ESSs integrated into EV charging stations help mitigate the adverse impacts of fast EV charging such as increased power losses and voltage drops in distribution networks. Additionally, optimal EMS decisions for fast EV charging stations are communicated to the VVO program, enabling it to leverage the active-reactive power (*P*-*Q*) capability of inverters for enhanced grid support. Reference [10] focuses on day-ahead operational scheduling, leveraging active and reactive vehicle-to-grid (V2G) capabilities of EV chargers to enhance voltage regulation and achieve energy savings. As proposed in [11], the joint implementation of integrated EMS and VVO programs enhances the performance of voltage regulation by coordinating inverter-based PV units, ESSs, and the integrated flexibility of heating, ventilation, air conditioning, and EV charging stations in commercial buildings.

Other studies have primarily focused on integrating VVO and EMS to enhance voltage regulation and operational efficiency, while neglecting the influence of EV charging stations. A two-stage framework combining demand-response programs and VVO is presented in [12], optimizing losses, voltages, and operational costs through multi-timescale coordination in networks with PV units and flexible impedance-current-power (ZIP) loads. A two-stage mixed-integer second-order cone programming (MISOCP) model is proposed in [13] to coordinate OLTCs, reactive compensators, and ESSs for minimizing losses, electricity costs, and wind power curtailment under constant power loads. In [14], a mixed-integer linear programming (MILP)-based RT voltage control framework is proposed to coordinate OLTCs and distributed generation and energy resources, aiming to maximize the revenue of utility from active power generation. Reference [15] introduces a mixed-integer nonlinear programming-based RT VVO scheme that aggregates PV units and ESSs as virtual power plants to minimize voltage deviation, system losses, and PV curtailment in sub-transmission networks. A two-stage mixed-integer nonlinear programming model based on a voltage-load sensitivity matrix is proposed in [16], using PV units and capacitors to reduce voltage deviations and demand-response costs in the first stage, followed by corrective actions in the second stage. In [17], a quadratic programming-based predictive voltage control strategy coordinates reactive compensators, OLTCs, and PV units under exponential load models to maintain voltage limits and enhance energy efficiency through demand-response and conservative voltage reduction. Further contributions integrate conservative voltage reduction and demand-response programs within an MISOCP model to minimize day-ahead electricity costs under exponential and ZIP loads [18]. MILP-based frameworks have also been developed for VVO, coordinating distributed generation and traditional voltage devices to minimize operational costs and voltage deviations under constant power loads [19], or to jointly optimize static voltage regulators, PV units, and ESSs for reducing line losses and electricity costs under ZIP load models [20].

Due to the variability in renewable power generation [6], [10]-[22], energy prices [9], [21]-[22], technical aspects of EVs (e. g., arrival time, state of charge, and charging power level) [8]-[11], and load [6], [9]-[13], [17], [22], decisions made by the integrated EMS and VVO applications are typically subject to uncertainties. To handle these uncertainties, deterministic optimization [6], [8], [13], [15]-[17], [19], [20], stochastic programming (SP) [6], [10], [18], chance-constrained (CC) optimization [11], [12], and robust optimization (RO) [9], [13], [14], [19] are commonly employed. Unlike deterministic approaches, SP effectively maintains voltage within admissible limits under PV and load fluctuations, albeit with slightly higher power losses and energy purchase costs [6]. The adaptive RO (ARO) approach provides economic advantages over deterministic approaches in terms of both worst-case and average performance [13]. Reference [19] reports the RT operational capabilities of both deterministic and RO approaches. Among various energy schedules of ADNs made by the EMS, energy trading is crucial from both economic and technical perspectives. However, the interdependence between energy trading and voltage control remains a primary concern. Similar to this paper, [21] and [22] also address this issue. Using a two-stage deterministic optimization model proposed in [21], the considered ADN leverages price-responsive demands, inverter-based PV units, and battery ESSs to participate in the RT energy market. It is reported in [21] that increased profit in the RT market comes at the expense of greater voltage violations. Reference [22] introduces a deterministic optimization framework in which the EV aggregator coordinates short-term charging and discharging operations of EVs with the system operator to ensure compliance with voltage constraints. After anticipating the active and reactive power requirements of EVs, the aggregator can engage in profitable energy trading within the day-ahead energy market. A key limitation of the deterministic approaches in [21] and [22] is the representation of uncertainty using a single-scenario forecast. Despite being simple and fast to implement, relying on a single scenario reduces accuracy and increases the risk of large errors. Consequently, any deviation between the actual realizations of uncertain parameters and the forecast can undermine the performance of decisions under the deterministic approach, both in terms of optimality and feasibility, introducing significant technical and financial risks. This concern becomes particularly critical when the operation of ADN is subject to higher uncertainty.

This paper aims to model the operation of ADN that can strategically participate in the RT energy market. The ADN includes flexible demands, EV charging stations, and PV units interconnected through a distribution network. Each EV charging station is equipped with a hybrid PV unit and ESS, allowing it to inject power to or absorb power from the network through a smart inverter. The integrated EMS and VVO programs determine the energy schedules and control device settings in a two-stage sequence. In the first stage, hourly decisions are made regarding the strategic offering of price-power quantity pairs in the RT energy market. Schedules for flexible demands and slow-acting devices are also determined, considering uncertainties in market prices, PV power generation, and EV charging levels. An ARO model is proposed to handle these uncertainties, which is solved using the column-and-constraint generation (CCG) algorithm. In the second stage, once the uncertain data are realized, fast-acting devices are controlled on a minute-by-minute basis. Out-of-sample analysis, conducted through a realistic case study, demonstrates how the ADN balances market participation with grid operational objectives.

As shown in Table I, a key knowledge gap in current studies [6], [8]-[22] lies in the modeling of operation of ADNs in RT energy markets. Although studies such as [21] and [22] have addressed this gap using deterministic approaches, further research is needed to incorporate advanced approaches for effectively handling uncertainty and enhancing the reliability of operations of ADNs in RT energy markets. Note that in Table I, Det represents deterministic; and √ and × represent considered and not considered, respectively.

TABLE I
COMPARISON OF THIS PAPER AND RELATED STUDIES

Reference	EV charging station			Uncertainty model	Uncertain data				Market
	PV	EV	ESS		DG	Price	EV	Load	
[6]	×	×	×	Det&SP	√	×	×	√	×
[8]	×	√	×	Det	×	×	√	×	×
[9]	×	√	√	RO	×	√	√	√	×
[10]	×	√	×	SP	√	×	√	√	×
[11]	×	√	×	CC	√	×	√	√	×
[12]	×	×	×	CC	√	×	×	√	×
[13]	×	×	×	Det&ARO	√	×	×	√	×
[14]	×	×	×	RO	√	×	×	×	×
[15], [16]	×	×	×	Det	√	×	×	×	×
[17]	×	×	×	Det	√	×	×	√	×
[18]	×	×	×	SP	√	×	×	√	×
[19]	×	×	×	Det&ARO	√	×	×	√	×
[20]	×	×	×	Det	×	×	×	×	×
[21]	×	×	×	Det	√	√	×	√	√
[22]	×	√	×	Det	√	√	×	√	√
This paper	√	√	√	Det&ARO	√	√	√	×	√

Within this context, the contributions of this paper are fourfold.

1) An ARO model for the operation of ADN in the RT energy market is proposed, which enables the integrated EMS and VVO programs to coordinate and optimize the schedules of electricity assets and energy trading in the market.

2) The capabilities of market trading, PV units, flexible demands, and EV charging stations are leveraged, while handling the associated uncertainties. In particular, the integrated operation of EVs, PV units, and ESSs located at each EV charging station is considered.

3) Through out-of-sample simulation, this paper analyzes how the uncertainty budget and penalty factor for voltage violations affect techno-economic metrics.

4) The performance of Det&ARO in terms of actual profits, voltage violations, and energy losses is compared, and their respective benefits for the operation of ADN in the RT energy market are evaluated.

The remainder of this paper is organized as follows. Section II presents the problem description, by explaining the operation of the integrated EMS and VVO programs. Section III formulates the energy scheduling of the ADN in the RT energy market as a deterministic optimization model, which is transformed into a min-max-min problem, i.e., the proposed model in Section IV. Section V presents the results of case study and their sensitivity analysis with respect to the risk strategy and penalty factor for voltage violations. Finally, Section VI concludes this paper.

II. Problem Description

A. ADN

The considered ADN includes flexible demands, PV units, and EV charging stations, which are interconnected through a balanced distribution network connected to the main grid. Each EV charging station is equipped with an on-site hybrid PV unit and ESS to charge the EVs. The flexible demands are price-responsive and voltage-dependent, and their loads are scheduled under demand-response programs. Additionally, OLTCs and capacitors in the ADN can be used to control the voltage throughout the distribution network.

A fundamental requirement for implementing the integrated computation in the considered ADN is smart grid technology, which enables the bidirectional communication between the integrated EMS and VVO programs and the RT energy market, as well as between the integrated EMS and VVO programs and the electricity assets.

B. RT Energy Market

To maximize profits, the ADN seeks to participate in the RT energy market. In this setting, the ADN submits offers of price-power quantity pairs at regular intervals (e.g., minute by minute) prior to market closure, while facing uncertainty in market prices. The market operator then conducts a security-constrained economic dispatch to clear the RT energy market, ensuring a balance between generation and demand at each bus in the transmission system, which is connected to the ADN through a number of buses. Once cleared, the ADN is informed of the accepted energy sold or purchased and the market price in each trading interval. This process aligns with the structure of many RT energy markets worldwide such as the Pennsylvania-New Jersey-Maryland (PJM) market in USA [23].

C. Operational Decision-making Sequence

The ADN operates within slow and fast timescales, which are described as follows.

1) In the slow timescale (e.g., hourly), the integrated EMS and VVO programs determine the coordinated offering curve and volt-var decisions hourly. The ADN can buy or sell energy by submitting price-power quantity pairs in the hourly RT energy market. Additionally, the active and reactive power levels of flexible demands are scheduled, and the settings of slow-acting devices (e.g., OLTCs and capacitors) are adjusted. These hourly decisions aim to maximize the profit while minimizing the voltage violations relative to admissible limits. The integrated EMS and VVO programs must address uncertainty in RT energy market prices, available PV power generation, and EV charging power levels. Effective uncertainty-handling approaches are therefore essential.

2) In the fast timescale (e.g., 15 min), the ADN operates over multiple time slots within each hour. Once the energy market is cleared, the ADN is informed of the market price and the traded power for the upcoming hour. Additionally, the available PV power generation and the charging active power levels of EVs are known for the upcoming hour with higher certainty. Using this updated information, the integrated EMS and VVO programs dispatch and adjust fast-acting devices such as PV units and EV charging stations, while considering voltage-dependent loads to improve the voltage profile and reduce power losses.

The step-by-step decisions made by the integrated EMS and VVO programs are described as follows.

1) The integrated EMS and VVO programs receive the technical and economic characteristics of electricity assets such as the minimum/maximum active power levels of flexible demands and their utility over the scheduling horizon $[\tau, T]$, as well as the initial energy levels of ESSs.

2) Forecasts of uncertain data including market prices, available active power from PV units, and EV charging active power levels are prepared for the scheduling horizon $[\tau, T]$.

3) The integrated EMS and VVO programs submit price-power quantity pairs in the hourly RT energy market. Additionally, flexible demands and slow-acting devices are scheduled.

4) Once the hourly RT energy market is cleared, the ADN is informed of the market price and its scheduled energy at hour τ. The actual realizations of uncertain data at hour τ are also observed.

5) Fast-acting devices are dispatched at regular intervals (e.g., every 15 min) at hour τ.

6) If $\tau < T$, then $\tau \leftarrow \tau + 1$; otherwise, the scheduling process is complete.

III. Deterministic Optimization Model

In this section, the optimal scheduling problem of the ADN for decision-making at hour τ in the RT energy market is formulated as a deterministic optimization problem using an MISOCP model.

A. Objective Function

The objective function of the ADN scheduling problem is formulated as:

$$\max\left\{\sum_{t=\tau}^{T}\left(\sum_{d\in\Omega^{\mathrm{D}}} U_{d,t}^{\mathrm{D}} p_{d,t}^{\mathrm{D}} \Delta_t + \sum_{s\in\Omega^{\mathrm{S}}} U_{s,t}^{\mathrm{EV,C}} \overline{P}_{s,t}^{\mathrm{EV,C}} \Delta_t - \lambda_t^{\mathrm{RT}} p_t^{\mathrm{M}} \Delta_t\right) - \omega\epsilon\right\} \tag{1}$$

The set $\Phi^{\mathrm{X}} = \{p_t^{\mathrm{M}},\ \forall t\in\Omega_\tau^{\mathrm{T}};\ q_{c,t}^{\mathrm{CAP}},\ \forall c\in\Omega^{\mathrm{C}},\ t\in\Omega_\tau^{\mathrm{T}};\ p_{d,t}^{\mathrm{D,S}},\ q_{d,t}^{\mathrm{D,S}},\ \forall d\in\Omega^{\mathrm{D}},\ t\in\Omega_\tau^{\mathrm{T}};\ r_{o,p,t}^{\mathrm{O,T}},\ \forall o\in\Omega^{\mathrm{O}},\ p\in\Omega_o^{\mathrm{O,T}},\ t\in\Omega_\tau^{\mathrm{T}};\ s_{c,t}^{\mathrm{CAP}},\ \forall c\in\Omega^{\mathrm{C}},\ t\in\Omega_\tau^{\mathrm{T}}\}$ includes the first-stage continuous and binary decision variables; and the set $\Phi^{\mathrm{Y}} = \{\epsilon;\ l_{bl,t},\ p_{bl,t}^{\mathrm{L}},\ q_{bl,t}^{\mathrm{L}},\ \forall(b,l)\in\Omega^{\mathrm{L}},\ \forall t\in\Omega_\tau^{\mathrm{T}};\ p_{d,t}^{\mathrm{D}},\ q_{d,t}^{\mathrm{D}},\ \forall d\in\Omega^{\mathrm{D}},\ t\in\Omega_\tau^{\mathrm{T}};\ p_{b,t}^{\mathrm{MG}},\ q_{b,t}^{\mathrm{MG}},$

$\forall b \in \Omega^{\mathrm{MG}}, \ \forall t \in \Omega_{\tau}^{\mathrm{T}}; p_{g,t}^{\mathrm{PV}}, \ q_{g,t}^{\mathrm{PV}}, \ \forall g \in \Omega^{\mathrm{PV}}, \ t \in \Omega_{\tau}^{\mathrm{T}}; e_{s,t}^{\mathrm{ST}}, \ p_{s,t}^{\mathrm{PV,S}}, \ p_{s,t}^{\mathrm{S}}, \ q_{s,t}^{\mathrm{S}}, \ p_{s,t}^{\mathrm{ST,C}}, \ p_{s,t}^{\mathrm{ST,D}}, \ \forall s \in \Omega^{\mathrm{S}}, \ t \in \Omega_{\tau}^{\mathrm{T}}; u_{b,t}, \ \overline{\Delta v}_{b,t}, \ \underline{\Delta v}_{b,t}, \forall b \in \Omega^{\mathrm{B}}, \ \forall t \in \Omega_{\tau}^{\mathrm{T}} \}$ includes the second-stage decision variables.

The objective function (1) aims to maximize the profit of the ADN while minimizing voltage violations over the scheduling horizon $[\tau, T]$. The first and second terms of the objective function represent the utility of energy consumption by flexible demands and the revenue obtained from charging EVs at the EV charging stations, respectively. Note that the revenue from selling energy to EVs is constant and can therefore be omitted. The third term corresponds to the cost or revenue resulting from buying or selling energy in the RT energy market. The final term penalizes voltage violations, weighted by the nonnegative value of ω.

B. Constraints

The objective function is subject to the feasible operational regions of market trading, distribution networks, OLTCs, capacitors, PV units, EV charging stations, and flexible demands, as detailed below.

$$p_t^{\mathrm{M}} = \sum_{b \in \Omega^{\mathrm{MG}}} p_{b,t}^{\mathrm{MG}} \quad \forall t \in \Omega_{\tau}^{\mathrm{T}} \tag{2}$$

$$-\overline{P}^{\mathrm{M}} \leq p_t^{\mathrm{M}} \leq \overline{P}^{\mathrm{M}} \quad \forall t \in \Omega_{\tau}^{\mathrm{T}} \tag{3}$$

Equation (2) calculates the power traded in the RT energy market as the sum of power injections at the buses connected to the main grid. The traded power is further bounded by the constraint in (3).

$$\epsilon = \sum_{t=\tau}^{T} \left[\sum_{b \in \Omega^{\mathrm{B}}} \left(\underline{\Delta v}_{b,t} + \overline{\Delta v}_{b,t} \right) \Delta_t \right] \tag{4}$$

Equation (4) computes total voltage violation over all buses during the scheduling horizon.

$$u_{l,t} = u_{b,t} - 2\left(R_{bl} p_{bl,t}^{\mathrm{L}} + X_{bl} q_{bl,t}^{\mathrm{L}} \right) + \left(R_{bl}^2 + X_{bl}^2 \right) l_{bl,t} \quad \forall (b,l) \in \Omega^{\mathrm{L}}, \forall t \in \Omega_{\tau}^{\mathrm{T}} \tag{5}$$

$$p_{b,t}^{\mathrm{MG}} + \sum_{(k,b) \in \Omega^{\mathrm{L}}} \left(p_{kb,t}^{\mathrm{L}} - R_{kb} l_{kb,t} \right) - \sum_{(b,l) \in \Omega^{\mathrm{L}}} p_{bl,t}^{\mathrm{L}} = \sum_{d \in \Omega_b^{\mathrm{D}}} p_{d,t}^{\mathrm{D}} \quad \forall b \in \Omega^{\mathrm{MG}}, \forall t \in \Omega_{\tau}^{\mathrm{T}} \tag{6}$$

$$\sum_{(k,b) \in \Omega^{\mathrm{L}}} \left(p_{kb,t}^{\mathrm{L}} - R_{kb} l_{kb,t} \right) - \sum_{(b,l) \in \Omega^{\mathrm{L}}} p_{bl,t}^{\mathrm{L}} + \sum_{g \in \Omega_b^{\mathrm{PV}}} p_{g,t}^{\mathrm{PV}} + \sum_{s \in \Omega_b^{\mathrm{S}}} p_{s,t}^{\mathrm{S}} = \sum_{d \in \Omega_b^{\mathrm{D}}} p_{d,t}^{\mathrm{D}} \quad \forall b \in \Omega^B \backslash \Omega^{\mathrm{MG}}, \forall t \in \Omega_{\tau}^{\mathrm{T}} \tag{7}$$

$$q_{b,t}^{\mathrm{MG}} + \sum_{(k,b) \in \Omega^{\mathrm{L}}} \left(q_{kb,t}^{\mathrm{L}} - X_{kb} l_{kb,t} \right) - \sum_{(b,l) \in \Omega^{\mathrm{L}}} q_{bl,t}^{\mathrm{L}} + \sum_{c \in \Omega_b^{\mathrm{C}}} q_{c,t}^{\mathrm{CAP}} = \sum_{d \in \Omega_b^{\mathrm{D}}} q_{d,t}^{\mathrm{D}} \quad \forall b \in \Omega^{\mathrm{MG}}, \forall t \in \Omega_{\tau}^{\mathrm{T}} \tag{8}$$

$$\sum_{(k,b) \in \Omega^{\mathrm{L}}} \left(q_{kb,t}^{\mathrm{L}} - X_{kb} l_{kb,t} \right) - \sum_{(b,l) \in \Omega^{\mathrm{L}}} q_{bl,t}^{\mathrm{L}} + \sum_{c \in \Omega_b^{\mathrm{C}}} q_{c,t}^{\mathrm{CAP}} + \sum_{g \in \Omega_b^{\mathrm{PV}}} q_{g,t}^{\mathrm{PV}} + \sum_{s \in \Omega_b^{\mathrm{S}}} q_{s,t}^{\mathrm{S}} = \sum_{d \in \Omega_b^{\mathrm{D}}} q_{d,t}^{\mathrm{D}} \quad \forall b \in \Omega^B \backslash \Omega^{\mathrm{MG}}, \forall t \in \Omega_{\tau}^{\mathrm{T}} \tag{9}$$

$$\left\| \left[2p_{bl,t}^{\mathrm{L}} \quad 2q_{bl,t}^{\mathrm{L}} \quad l_{bl,t} - u_{b,t} \right]^{\mathrm{T}} \right\|_2 \leq l_{bl,t} + u_{b,t} \quad \forall (b,l) \in \Omega^{\mathrm{L}}, \forall t \in \Omega_{\tau}^{\mathrm{T}} \tag{10}$$

$$l_{bl,t} \leq \overline{I}_{bl}^2 \quad \forall (b,l) \in \Omega^{\mathrm{L}}, \forall t \in \Omega_{\tau}^{\mathrm{T}} \tag{11}$$

$$\underline{V}_b^2 - \underline{\Delta v}_{b,t} \leq u_{b,t} \leq \overline{V}_b^2 + \overline{\Delta v}_{b,t} \quad \forall b \in \Omega^{\mathrm{B}}, \forall t \in \Omega_{\tau}^{\mathrm{T}} \tag{12}$$

$$\left\| \left[p_{b,t}^{\mathrm{MG}} \quad q_{b,t}^{\mathrm{MG}} \right]^{\mathrm{T}} \right\|_2 \leq \overline{S}_b^{\mathrm{MG}} \quad \forall b \in \Omega^{\mathrm{MG}}, \forall t \in \Omega_{\tau}^{\mathrm{T}} \tag{13}$$

$$p_{d,t}^{\mathrm{D}} = p_{d,t}^{\mathrm{D,S}} \left(\alpha_{d,t}^{\mathrm{Z}} u_{b|d \in \Omega_b^{\mathrm{D}},t} + \alpha_{d,t}^{\mathrm{P}} \right) \quad \forall d \in \Omega^{\mathrm{D}}, \forall t \in \Omega_{\tau}^{\mathrm{T}} \tag{14}$$

$$q_{d,t}^{\mathrm{D}} = q_{d,t}^{\mathrm{D,S}} \left(\beta_{d,t}^{\mathrm{Z}} u_{b|d \in \Omega_b^{\mathrm{D}},t} + \beta_{d,t}^{\mathrm{P}} \right) \quad \forall d \in \Omega^{\mathrm{D}}, \forall t \in \Omega_{\tau}^{\mathrm{T}} \tag{15}$$

Constraints (5)-(15) are the technical limitations of the power grid including the conic relaxation of power flow equations (5)-(10), lines capacity (11), admissible range of voltage (12) considering any deviations, apparent power capacity of main grid connections (13), the impedance-power (ZP) model of active and reactive power loads (14) and (15), respectively. Although the ZIP model more accurately represents load behavior, it introduces non-convexity and nonlinearity, increasing computational complexity and often preventing timely convergence. Thus, the ZP model serves as a practical approximation [24], ensuring adequate and efficient performance in RT operation.

$$u_{b|o \in \Omega_b^{\mathrm{O}},t} = V_{0,t}^2 \sum_{p \in \Omega_o^{\mathrm{O,T}}} r_{o,p,t}^{\mathrm{O,T}} X_{o,p}^{\mathrm{O,T}} \quad \forall o \in \Omega^{\mathrm{O}}, \forall t \in \Omega_{\tau}^{\mathrm{T}} \tag{16}$$

$$\sum_{p \in \Omega_o^{\mathrm{O,T}}} r_{o,p,t}^{\mathrm{O,T}} = 1 \quad \forall o \in \Omega^{\mathrm{O}}, \forall t \in \Omega_{\tau}^{\mathrm{T}} \tag{17}$$

Equations (16) and (17) implement the function of the OLTC and make the relationship between input and output voltages based on the active position of tap.

$$q_{c,t}^{\mathrm{CAP}} = s_{c,t}^{\mathrm{CAP}} \overline{Q}_c^{\mathrm{CAP}} \quad \forall c \in \Omega^{\mathrm{C}}, \forall t \in \Omega_{\tau}^{\mathrm{T}} \tag{18}$$

Constraint (18) shows the reactive power injected by capacitors according to their status.

$$0 \leq p_{g,t}^{\mathrm{PV}} \leq \overline{P}_{g,t}^{\mathrm{PV}} \quad \forall g \in \Omega^{\mathrm{PV}}, \forall t \in \Omega_{\tau}^{\mathrm{T}} \tag{19}$$

$$-p_{g,t}^{\mathrm{PV}} \sqrt{\frac{1}{\left(\underline{PF}_g^{\mathrm{PV}} \right)^2} - 1} \leq q_{g,t}^{\mathrm{PV}} \leq p_{g,t}^{\mathrm{PV}} \sqrt{\frac{1}{\left(\underline{PF}_g^{\mathrm{PV}} \right)^2} - 1} \quad \forall g \in \Omega^{\mathrm{PV}}, t \in \Omega_{\tau}^{\mathrm{T}} \tag{20}$$

$$\left\| \left[p_{g,t}^{\mathrm{PV}} \quad q_{g,t}^{\mathrm{PV}} \right]^{\mathrm{T}} \right\|_2 \leq \overline{S}_g^{\mathrm{PV}} \quad \forall g \in \Omega^{\mathrm{PV}}, \forall t \in \Omega_{\tau}^{\mathrm{T}} \tag{21}$$

Equations (19)-(21) govern the operation of PV units, considering the upper bound on available active power generation (19), the limitation on reactive power injection (20) imposed by the minimum power factor, and the apparent power capacity of the inverter (21).

$$p_{s,t}^{\mathrm{S}} = p_{s,t}^{\mathrm{PV,S}} + p_{s,t}^{\mathrm{ST,D}} - p_{s,t}^{\mathrm{ST,C}} - \overline{P}_{s,t}^{\mathrm{EV,C}} \quad \forall s \in \Omega^{\mathrm{S}}, \forall t \in \Omega_{\tau}^{\mathrm{T}} \tag{22}$$

$$0 \leq p_{s,t}^{\mathrm{PV,S}} \leq \overline{P}_{s,t}^{\mathrm{PV,S}} \quad \forall s \in \Omega^{\mathrm{S}}, \forall t \in \Omega_{\tau}^{\mathrm{T}} \tag{23}$$

$$0 \leq p_{s,t}^{\mathrm{ST,C}} \leq \overline{P}_s^{\mathrm{ST,C}} \quad \forall s \in \Omega^{\mathrm{S}}, \forall t \in \Omega_{\tau}^{\mathrm{T}} \tag{24}$$

$$0 \leq p_{s,t}^{\mathrm{ST,D}} \leq \overline{P}_s^{\mathrm{ST,D}} \quad \forall s \in \Omega^{\mathrm{S}}, \forall t \in \Omega_{\tau}^{\mathrm{T}} \tag{25}$$

$$e_{s,t}^{\mathrm{ST}} = e_{s,t-1}^{\mathrm{ST}} + \Delta_t \left(p_{s,t}^{\mathrm{ST,C}} \eta_s^{\mathrm{ST,C}} - \frac{p_{s,t}^{\mathrm{ST,D}}}{\eta_s^{\mathrm{ST,D}}} \right) \quad \forall s \in \Omega^{\mathrm{S}}, \forall t \in \Omega_{\tau}^{\mathrm{T}} \tag{26}$$

$$\underline{E}_s^{\mathrm{ST}} \leq e_{s,t}^{\mathrm{ST}} \leq \overline{E}_s^{\mathrm{ST}} \quad \forall s \in \Omega^{\mathrm{S}}, \forall t \in \Omega_{\tau}^{\mathrm{T}} \tag{27}$$

$$\underline{Q}_s^{\mathrm{S}} \leq q_{s,t}^{\mathrm{S}} \leq \overline{Q}_s^{\mathrm{S}} \quad \forall s \in \Omega^{\mathrm{S}}, \forall t \in \Omega_\tau^{\mathrm{T}} \tag{28}$$

$$\left\| \left[p_{s,t}^{\mathrm{S}} \quad q_{s,t}^{\mathrm{S}} \right]^{\mathrm{T}} \right\|_2 \leq \overline{S}_s^{\mathrm{S}} \quad \forall s \in \Omega^{\mathrm{S}}, \forall t \in \Omega_\tau^{\mathrm{T}} \tag{29}$$

Constraints (22)-(29) define the feasible operational region of each EV charging station. This includes the active power balance (22), active power generation from its PV unit (23), and the charging and discharging power limits of its ESS (24) and (25), respectively. The energy evolution of the ESS is described in (26) and bounded by (27). Additionally, the constraints account for the reactive power injection (28) and the apparent power capacity of the inverter (29).

$$\underline{P}_{d,t}^{\mathrm{D}} \leq p_{d,t}^{\mathrm{D,S}} \leq \overline{P}_{d,t}^{\mathrm{D}} \quad \forall d \in \Omega^{\mathrm{D}}, \forall t \in \Omega_\tau^{\mathrm{T}} \tag{30}$$

$$q_{d,t}^{\mathrm{D,S}} = p_{d,t}^{\mathrm{D,S}} \sqrt{\frac{1}{\left(PF_d^{\mathrm{D}}\right)^2} - 1} \quad \forall d \in \Omega^{\mathrm{D}}, \forall t \in \Omega_\tau^{\mathrm{T}} \tag{31}$$

$$-R_d^{\mathrm{D,D}} \leq p_{d,t}^{\mathrm{D,S}} - p_{d,(t-1)}^{\mathrm{D,S}} \leq R_d^{\mathrm{D,U}} \quad \forall d \in \Omega^{\mathrm{D}}, \forall t \in \Omega_\tau^{\mathrm{T}} \tag{32}$$

Constraints (30) - (32) are the limitations of flexible demands including the scheduled active and reactive power load (30) and (31), respectively, and their pick-up/drop ramping limit (32).

Constraints (14) and (15) involve the multiplication of two continuous variables, $p_{d,t}^{\mathrm{D,S}}$ and $u_{b|d \in \Omega_b^{\mathrm{D}},t}$, as well as $q_{d,t}^{\mathrm{D,S}}$ and $u_{b|d \in \Omega_b^{\mathrm{D}},t}$, which renders the optimization problem nonlinear. This nonlinearity can be linearized using the methodology in [25]. In this way, the nonlinear problem (1) - (32) is transformed into an MISOCP, ensuring its optimality [6].

IV. Proposed Model

A. Uncertainty Set

Through the ARO, the uncertain data of RT energy market price λ_t^{RT}, PV power generations $\overline{P}_{g,t}^{\mathrm{PV}}$, $\overline{P}_{s,t}^{\mathrm{PV,S}}$, and charging active power level of EVs $\overline{P}_{s,t}^{\mathrm{EV,C}}$ are presented by the uncertainty set. In general form, the uncertainty set Λ^{U} defines the uncertain data as a set of decision variables $u \in \Phi^{\mathrm{U}} = \left\{\lambda_t^{\mathrm{RT}}, \overline{P}_{g,t}^{\mathrm{PV}}, \overline{P}_{s,t}^{\mathrm{PV,S}}, \overline{P}_{s,t}^{\mathrm{EV,C}}\right\}$, which are constrained by predicted confidence bounds, e.g., $u_t \in \left[\tilde{u}_t - \hat{u}_t, \tilde{u}_t + \hat{u}_t\right]$, $\forall t$, for a given confidence level and a chosen uncertainty budget, where u_t is an uncertain variable; and $\tilde{u}_t$ and $\hat{u}_t$ are the average value and fluctuation level of u_t associated with the corresponding confidence bounds, respectively. A polyhedral uncertainty set can be formed by the general MILP formulation as:

$$\Lambda^{\mathrm{U}} = \left\{u_t \middle| \underline{k}_t, \overline{k}_t \in \{0,1\}\right\} \quad \forall t \tag{33}$$

$$u_t = \tilde{u}_t - \underline{k}_t \hat{u}_t + \overline{k}_t \hat{u}_t \quad \forall t \tag{34}$$

$$\underline{k}_t + \overline{k}_t \leq 1 \quad \forall t \tag{35}$$

$$\sum_t \left(\underline{k}_t + \overline{k}_t\right) \leq \Gamma \tag{36}$$

The binary variables $\underline{k}_t$ and $\overline{k}_t$ in (33) are used to model deviations from the average value of a parameter. Equation (34) expresses the value of u_t in terms of $\tilde{u}_t$ and $\hat{u}_t$. Equation (35) ensures that an uncertain variable does not simultaneously take its minimum and maximum bounds. Equation (36) controls the conservativeness of the model through the uncertainty budget Γ, which defines a cardinality-constrained uncertainty set as introduced in [26]. This parameter limits the number of uncertain variables allowed to deviate from their nominal values and enables a trade-off between robustness and performance. Γ is a nonnegative scalar, with its maximum value equal to the total number of uncertain parameters.

In the ADN scheduling problem, the integrated EMS and VVO programs face uncertain data over the scheduling horizon $[\tau, T]$. In this case, the uncertainty set defined by (33)-(36) is time-dependent. Accordingly, the uncertainty budget can take values between 0 and $\left|\Omega_\tau^{\mathrm{T}}\right|$.

B. Proposed Model

Given the uncertainty set (33), the scheduling model (1)-(32) can be transformed into the proposed model for making decisions at hour τ as:

$$\min_{\Phi^{\mathrm{X}}} \max_{\Phi^{\mathrm{U}}} \min_{\Phi^{\mathrm{Y}}} (1) \tag{37}$$

s.t.

$$(3), (17), (18), (30), (32) \tag{38}$$

$$\Phi^{\mathrm{U}} \in \Lambda^{\mathrm{U}} \tag{39}$$

$$(2), (4)\text{-}(16), (19)\text{-}(29) \tag{40}$$

In the ARO, the deterministic model (1)-(32) is reformulated into a tri-level optimization model (37)-(40). The upper-level problem minimizes the worst-case optimal operational cost over the scheduling decisions $\boldsymbol{x} \in \Phi^{\mathrm{X}}$. Constraint (38) defines the feasible operational region for these decisions, considering the limits of energy trading in the RT market (3), the settings of OLTCs (17), the status of capacitors (18), and the technical limitations of flexible demands (30)-(32). For a given upper-level decision, the middle-level problem determines the worst-case realization of the uncertainty variables $\boldsymbol{u} \in \Phi^{\mathrm{U}}$ within the predefined uncertainty set Λ^{U}. The lower-level problem determines the optimal dispatch decisions $\boldsymbol{y} \in \Phi^{\mathrm{Y}}$ in response to the worst-case uncertainty identified in the middle-level problem. It is constrained by the feasible operational region of the ADN, which is defined by active power exchange with the main grid (2), bus voltage violation (4), technical constraints of the electric network (5)-(16), active and reactive power limits of PV units (19)-(21), and the power and energy limits of EV charging stations (22)-(29).

In the proposed model, let $\boldsymbol{x}$, $\boldsymbol{u}$, and $\boldsymbol{y}$ represent upper- (both continuous and binary scheduling variables), middle- (uncertain variables), and lower-level (dispatch variables) variables at the upper-level problem, respectively. For the sake of clarity, the generalized formulation of ARO is provided as:

$$\min_{\boldsymbol{x} \in \Phi^{\mathrm{X}}} \max_{\boldsymbol{u} \in \Phi^{\mathrm{U}}} \min_{\boldsymbol{y} \in \Phi^{\mathrm{Y}}} \left(\boldsymbol{u}^{\mathrm{T}} \boldsymbol{F} \boldsymbol{x} + \boldsymbol{H} \boldsymbol{y}\right) \tag{41}$$

s.t.

$$\boldsymbol{A}\boldsymbol{x} = \boldsymbol{B} \tag{42}$$

$$\boldsymbol{A}'\boldsymbol{x} \leq \boldsymbol{B}' \tag{43}$$

$$\Phi^{\mathrm{U}} \in \Lambda^{\mathrm{U}} \tag{44}$$

$$\boldsymbol{Zy} \le \boldsymbol{Su} + \boldsymbol{W} \tag{45}$$

$$\boldsymbol{Z'y} = \boldsymbol{S'u} + \boldsymbol{W'x} \tag{46}$$

$$\left\| \boldsymbol{D}_{bl,t}^{\mathrm{L}} \boldsymbol{y} \right\|_2 \le \boldsymbol{J}_{bl,t}^{\mathrm{L}} \boldsymbol{y} \quad \forall (b,l) \in \Omega^{\mathrm{L}}, \forall t \in \Omega_\tau^{\mathrm{T}} \tag{47}$$

$$\left\| \boldsymbol{D}_{b,t}^{\mathrm{MG}} \boldsymbol{y} \right\|_2 \le \boldsymbol{C}_b^{\mathrm{MG}} \quad \forall b \in \Omega^{\mathrm{MG}}, \forall t \in \Omega_\tau^{\mathrm{T}} \tag{48}$$

$$\left\| \boldsymbol{D}_{g,t}^{\mathrm{PV}} \boldsymbol{y} \right\|_2 \le \boldsymbol{C}_g^{\mathrm{PV}} \quad \forall g \in \Omega^{\mathrm{PV}}, \forall t \in \Omega_\tau^{\mathrm{T}} \tag{49}$$

$$\left\| \boldsymbol{D}_{s,t}^{\mathrm{S}} \boldsymbol{y} \right\|_2 \le \boldsymbol{C}_s^{\mathrm{S}} \quad \forall s \in \Omega^{\mathrm{S}}, \forall t \in \Omega_\tau^{\mathrm{T}} \tag{50}$$

In above equations, the components $\boldsymbol{F}$, $\boldsymbol{H}$, $\boldsymbol{A}$, $\boldsymbol{B}$, $\boldsymbol{A'}$, $\boldsymbol{B'}$, $\boldsymbol{Z}$, $\boldsymbol{S}$, $\boldsymbol{W}$, $\boldsymbol{Z'}$, $\boldsymbol{S'}$, $\boldsymbol{W'}$, $\boldsymbol{D}_{bl,t}^{\mathrm{L}}$, $\boldsymbol{J}_{bl,t}^{\mathrm{L}}$, $\boldsymbol{D}_{b,t}^{\mathrm{MG}}$, $\boldsymbol{C}_b^{\mathrm{MG}}$, $\boldsymbol{D}_{g,t}^{\mathrm{PV}}$, $\boldsymbol{C}_g^{\mathrm{PV}}$, $\boldsymbol{D}_{s,t}^{\mathrm{S}}$, and $\boldsymbol{C}_s^{\mathrm{S}}$ are the known parameters of the proposed model.

The objective function (41) minimizes the worst-case operational cost of the ADN, defined as the cost of energy trading in the RT market ($\boldsymbol{u}^{\mathrm{T}}\boldsymbol{Fx}$) plus the dispatching cost (i.e., the penalty for voltage violations minus the revenue from selling energy to demands presented as the closed form of $\boldsymbol{Hy}$). The upper-level constraints depend solely on the scheduling decisions $\boldsymbol{x}$. Specifically, (42) includes the linear equality constraints (17), (18), and (31), while (43) captures the linear inequality constraints (3), (30), and (32). The middle-level equation (44) specifies the uncertainty set. Finally, the lower-level constraints (45)-(50) define the feasible operational region of the ADN as a function of $\boldsymbol{x}$, $\boldsymbol{u}$, and $\boldsymbol{y}$. Among these, (45) and (46) represent all linear inequality and equality constraints, respectively, while (47)-(50) represent the conic formulations of (10), (13), (21), and (29), respectively.

C. CCG Algorithm

The proposed model can be solved using a CCG algorithm [13], [27]. This algorithm iteratively solves a master problem and a subproblem, which interact by exchanging information about their decision variables. The lower and upper bounds of the objective function are obtained from the master problem and subproblem, respectively, and the iterations continue until the difference between these bounds satisfies a convergence criterion. The CCG algorithm guarantees convergence to the global optimum of the MISOCP [13], [27]. The generic formulations of the master problem and subproblem, along with the computational algorithm, are described in the following subsections. For clarity, a flowchart of the CCG algorithm is provided in Supplementary Material A Fig. SA1.

1) Master Problem

The master problem at iteration h is formulated as:

$$\min_{\Phi^{\mathrm{M}}} \rho \tag{51}$$

s.t.

$$\boldsymbol{Ax} = \boldsymbol{B} \tag{52}$$

$$\boldsymbol{A'x} \le \boldsymbol{B'} \tag{53}$$

$$\rho \ge \left(\boldsymbol{u}^{(h')} \right)^{\mathrm{T}} \boldsymbol{Fx} + \boldsymbol{Hy}_{h'} \quad \forall h' = 1, 2, ..., h-1 \tag{54}$$

$$\boldsymbol{Zy}_{h'} \le \boldsymbol{Su}^{(h')} + \boldsymbol{W} \quad \forall h' = 1, 2, ..., h-1 \tag{55}$$

$$\boldsymbol{Z'y}_{h'} = \boldsymbol{S'u}^{(h')} + \boldsymbol{W'x} \quad \forall h' = 1, 2, ..., h-1 \tag{56}$$

$$\left\| \boldsymbol{D}_{bl,t}^{\mathrm{L}} \boldsymbol{y}_{h'} \right\|_2 \le \boldsymbol{J}_{bl,t}^{\mathrm{L}} \boldsymbol{y} \quad \forall (b,l) \in \Omega^{\mathrm{L}}, \forall t \in \Omega_\tau^{\mathrm{T}}, \forall h' = 1, 2, ..., h-1 \tag{57}$$

$$\left\| \boldsymbol{D}_{b,t}^{\mathrm{MG}} \boldsymbol{y}_{h'} \right\|_2 \le \boldsymbol{C}_b^{\mathrm{MG}} \quad \forall b \in \Omega^{\mathrm{MG}}, \forall t \in \Omega_\tau^{\mathrm{T}}, \forall h' = 1, 2, ..., h-1 \tag{58}$$

$$\left\| \boldsymbol{D}_{g,t}^{\mathrm{PV}} \boldsymbol{y}_{h'} \right\|_2 \le \boldsymbol{C}_g^{\mathrm{PV}} \quad \forall g \in \Omega^{\mathrm{PV}}, \forall t \in \Omega_\tau^{\mathrm{T}}, \forall h' = 1, 2, ..., h-1 \tag{59}$$

$$\left\| \boldsymbol{D}_{s,t}^{\mathrm{S}} \boldsymbol{y}_{h'} \right\|_2 \le \boldsymbol{C}_s^{\mathrm{S}} \quad \forall s \in \Omega^{\mathrm{S}}, \forall t \in \Omega_\tau^{\mathrm{T}}, \forall h' = 1, 2, ..., h-1 \tag{60}$$

The variables in set $\Phi^{\mathrm{M}} = \left\{ \boldsymbol{x}; \rho; \boldsymbol{y}_{h'}, \forall h' = 1, 2, ..., h-1 \right\}$ are the optimization variables of a master problem. The master problem (51)-(60) is a relaxed version of the tri-level optimization problem (41)-(50), wherein the auxiliary variable ρ iteratively approximates the worst-case of the middle-level objective function. Parameter $\boldsymbol{u}^{(h')}$, denoting the optimal value of $\boldsymbol{u}$, is obtained from solving the subproblem at iteration h'.

2) Subproblem

The subproblem is a bi-level optimization problem corresponding to the middle and lower levels of the original ARO problem. It is parameterized by $\boldsymbol{x}^{(h)}$ obtained from solving the master problem (51)-(60) at iteration h. The formulation of the subproblem is given as:

$$\max_{\boldsymbol{u} \in \Phi^{\mathrm{U}}} \min_{\boldsymbol{y} \in \Phi^{\mathrm{Y}}} \left(\boldsymbol{u}^{\mathrm{T}} \boldsymbol{Fx}^{(h)} + \boldsymbol{Hy} \right) \tag{61}$$

s.t.

$$\Phi^{\mathrm{U}} \in \Lambda^{\mathrm{U}} \tag{62}$$

$$\boldsymbol{Zy} \le \boldsymbol{Su} + \boldsymbol{W} : \boldsymbol{\zeta} \tag{63}$$

$$\boldsymbol{Z'y} = \boldsymbol{S'u} + \boldsymbol{W'x}^{(h)} : \boldsymbol{\lambda} \tag{64}$$

$$\left\| \boldsymbol{D}_{bl,t}^{\mathrm{L}} \boldsymbol{y} \right\|_2 \le \boldsymbol{J}_{bl,t}^{\mathrm{L}} \boldsymbol{y} : \underline{\boldsymbol{\mu}}_{bl,t}^{\mathrm{L}}, \bar{\boldsymbol{\mu}}_{bl,t}^{\mathrm{L}} \quad \forall (b,l) \in \Omega^{\mathrm{L}}, \forall t \in \Omega_\tau^{\mathrm{T}} \tag{65}$$

$$\left\| \boldsymbol{D}_{b,t}^{\mathrm{MG}} \boldsymbol{y} \right\|_2 \le \boldsymbol{C}_b^{\mathrm{MG}} : \underline{\boldsymbol{\mu}}_{b,t}^{\mathrm{MG}}, \bar{\boldsymbol{\mu}}_{b,t}^{\mathrm{MG}} \quad \forall b \in \Omega^{\mathrm{MG}}, \forall t \in \Omega_\tau^{\mathrm{T}} \tag{66}$$

$$\left\| \boldsymbol{D}_{g,t}^{\mathrm{PV}} \boldsymbol{y} \right\|_2 \le \boldsymbol{C}_g^{\mathrm{PV}} : \underline{\boldsymbol{\mu}}_{g,t}^{\mathrm{PV}}, \bar{\boldsymbol{\mu}}_{g,t}^{\mathrm{PV}} \quad \forall g \in \Omega^{\mathrm{PV}}, \forall t \in \Omega_\tau^{\mathrm{T}} \tag{67}$$

$$\left\| \boldsymbol{D}_{s,t}^{\mathrm{S}} \boldsymbol{y} \right\|_2 \le \boldsymbol{C}_s^{\mathrm{S}} : \underline{\boldsymbol{\mu}}_{s,t}^{\mathrm{S}}, \bar{\boldsymbol{\mu}}_{s,t}^{\mathrm{S}} \quad \forall s \in \Omega^{\mathrm{S}}, \forall t \in \Omega_\tau^{\mathrm{T}} \tag{68}$$

where the dual variables are separated with a colon. Note that $\underline{\boldsymbol{\mu}}_{bl,t}^{\mathrm{L}}$, $\bar{\boldsymbol{\mu}}_{bl,t}^{\mathrm{L}}$, $\underline{\boldsymbol{\mu}}_{b,t}^{\mathrm{MG}}$, $\bar{\boldsymbol{\mu}}_{b,t}^{\mathrm{MG}}$, $\underline{\boldsymbol{\mu}}_{g,t}^{\mathrm{PV}}$, $\bar{\boldsymbol{\mu}}_{g,t}^{\mathrm{PV}}$, $\underline{\boldsymbol{\mu}}_{s,t}^{\mathrm{S}}$, and $\bar{\boldsymbol{\mu}}_{s,t}^{\mathrm{S}}$ are the conic dual variables for the second-order cone equations (65)-(68).

Subproblem (61)-(68) is a bi-level problem whose lower-level is a second-order cone program, and thus, the strong duality holds under sufficient conditions provided in [28]. Such a property allows to replace the lower-level problem with its equivalent dual problem, and convert the bi-level problem into an equivalent single-level problem as:

$$\max_{\Phi^{\mathrm{U}}, \Phi^{\mathrm{D}}} \alpha \tag{69}$$

s.t.

$$\alpha \le \boldsymbol{u}^{\mathrm{T}} \boldsymbol{Fx}^{(h)} + \left(\boldsymbol{Su} + \boldsymbol{W} \right)^{\mathrm{T}} \boldsymbol{\zeta} + \left(\boldsymbol{S'u} + \boldsymbol{W'x}^{(h)} \right)^{\mathrm{T}} \boldsymbol{\lambda} - \sum_{t \in \Omega_\tau^{\mathrm{T}}} \sum_{b \in \Omega^{\mathrm{MG}}} \boldsymbol{C}_b^{\mathrm{MG}} \bar{\boldsymbol{\mu}}_{b,t}^{\mathrm{MG}} - \sum_{t \in \Omega_\tau^{\mathrm{T}}} \sum_{g \in \Omega^{\mathrm{PV}}} \boldsymbol{C}_g^{\mathrm{PV}} \bar{\boldsymbol{\mu}}_{g,t}^{\mathrm{PV}} - \sum_{t \in \Omega_\tau^{\mathrm{T}}} \sum_{s \in \Omega^{\mathrm{S}}} \boldsymbol{C}_s^{\mathrm{S}} \bar{\boldsymbol{\mu}}_{s,t}^{\mathrm{S}} \tag{70}$$

$$\Phi^{\mathrm{U}} \in \Lambda^{\mathrm{U}} \tag{71}$$

$$\boldsymbol{Z}^{\mathrm{T}}\boldsymbol{\zeta}+\left(\boldsymbol{Z}'\right)^{\mathrm{T}}\boldsymbol{\lambda}+\sum_{t\in\Omega_\tau^{\mathrm{T}}}\sum_{(b,l)\in\Omega^{\mathrm{L}}}\left(\boldsymbol{D}_{bl,t}^{\mathrm{L}}\right)^{\mathrm{T}}\underline{\boldsymbol{\mu}}_{bl,t}^{\mathrm{L}}+ \sum_{t\in\Omega_\tau^{\mathrm{T}}}\sum_{(b,l)\in\Omega^{\mathrm{L}}}\left(\boldsymbol{J}_{bl,t}^{\mathrm{L}}\right)^{\mathrm{T}}\bar{\boldsymbol{\mu}}_{bl,t}^{\mathrm{L}}+\sum_{t\in\Omega_\tau^{\mathrm{T}}}\sum_{b\in\Omega^{\mathrm{MG}}}\left(\boldsymbol{D}_{b,t}^{\mathrm{MG}}\right)^{\mathrm{T}}\underline{\boldsymbol{\mu}}_{b,t}^{\mathrm{MG}}+ \sum_{t\in\Omega_\tau^{\mathrm{T}}}\sum_{g\in\Omega^{\mathrm{PV}}}\left(\boldsymbol{D}_{g,t}^{\mathrm{PV}}\right)^{\mathrm{T}}\underline{\boldsymbol{\mu}}_{g,t}^{\mathrm{PV}}+\sum_{t\in\Omega_\tau^{\mathrm{T}}}\sum_{s\in\Omega^{\mathrm{S}}}\left(\boldsymbol{D}_{s,t}^{\mathrm{S}}\right)^{\mathrm{T}}\underline{\boldsymbol{\mu}}_{s,t}^{\mathrm{S}}=\boldsymbol{H}^{\mathrm{T}}\!:\!\boldsymbol{y} \tag{72}$$

$$\left\|\underline{\boldsymbol{\mu}}_{bl,t}^{\mathrm{L}}\right\|_2\le\bar{\boldsymbol{\mu}}_{bl,t}^{\mathrm{L}}\quad\forall(b,l)\in\Omega^{\mathrm{L}},\forall t\in\Omega_\tau^{\mathrm{T}} \tag{73}$$

$$\left\|\underline{\boldsymbol{\mu}}_{b,t}^{\mathrm{MG}}\right\|_2\le\bar{\boldsymbol{\mu}}_{b,t}^{\mathrm{MG}}\quad\forall b\in\Omega^{\mathrm{MG}},\forall t\in\Omega_\tau^{\mathrm{T}} \tag{74}$$

$$\left\|\underline{\boldsymbol{\mu}}_{g,t}^{\mathrm{PV}}\right\|_2\le\bar{\boldsymbol{\mu}}_{g,t}^{\mathrm{PV}}\quad\forall g\in\Omega^{\mathrm{PV}},\forall t\in\Omega_\tau^{\mathrm{T}} \tag{75}$$

$$\left\|\underline{\boldsymbol{\mu}}_{s,t}^{\mathrm{S}}\right\|_2\le\bar{\boldsymbol{\mu}}_{s,t}^{\mathrm{S}}\quad\forall s\in\Omega^{\mathrm{S}},\forall t\in\Omega_\tau^{\mathrm{T}} \tag{76}$$

$$\boldsymbol{\lambda},\underline{\boldsymbol{\mu}}_{bl,t}^{\mathrm{L}},\underline{\boldsymbol{\mu}}_{b,t}^{\mathrm{MG}},\underline{\boldsymbol{\mu}}_{g,t}^{\mathrm{PV}},\underline{\boldsymbol{\mu}}_{s,t}^{\mathrm{S}}\text{:free},\boldsymbol{\zeta}\le 0,\bar{\boldsymbol{\mu}}_{bl,t}^{\mathrm{L}},\bar{\boldsymbol{\mu}}_{b,t}^{\mathrm{MG}},\bar{\boldsymbol{\mu}}_{g,t}^{\mathrm{PV}},\bar{\boldsymbol{\mu}}_{s,t}^{\mathrm{S}}\ge 0 \tag{77}$$

where $\Phi^{\mathrm{D}}=\left\{\boldsymbol{\zeta};\boldsymbol{\lambda};\ \underline{\boldsymbol{\mu}}_{bl,t}^{\mathrm{L}};\bar{\boldsymbol{\mu}}_{bl,t}^{\mathrm{L}};\ \underline{\boldsymbol{\mu}}_{b,t}^{\mathrm{MG}};\bar{\boldsymbol{\mu}}_{b,t}^{\mathrm{MG}};\ \underline{\boldsymbol{\mu}}_{g,t}^{\mathrm{PV}};\bar{\boldsymbol{\mu}}_{g,t}^{\mathrm{PV}};\ \underline{\boldsymbol{\mu}}_{s,t}^{\mathrm{S}};\bar{\boldsymbol{\mu}}_{s,t}^{\mathrm{S}}\right\}$ contains all dual variables.

The above problem includes nonlinear terms $(\boldsymbol{Su})^{\mathrm{T}}\boldsymbol{\zeta}$ and $(\boldsymbol{S'u})^{\mathrm{T}}\boldsymbol{\lambda}$ in constraint (70), which are linearized [29].

V. Case Study

A. Data

The integrated EMS and VVO programs are implemented in an ADN comprising 68 flexible demands, two PV units, and two EV charging stations, which are interconnected through a modified IEEE 69-bus test system, as shown in Supplementary Material A Fig. SA2. Detailed information of this test system is provided in [30]. In this case study, all variables and parameters are expressed in per-unit (p.u.) values using a base apparent power of 1 MVA and a base voltage of 10 kV. The distribution network supplies diverse commercial demands, including full-service restaurants, large hotels, quick-service restaurants, retail stand-alone stores, retail strip malls, and warehouses. These demands are located in Bristol, Virginia, USA, and their technical data are obtained from [31]. The active power levels are scaled to match the distribution network, ensuring a peak load of 5.2 p.u.. All demands are assumed to be price-responsive, with utility values ranging from 15 to 55 \$/MWh throughout the day. The parameters for the ZIP model of commercial demands are obtained from [32] and converted into equivalent ZP model coefficients using the formulation proposed in [24].

Bus 1 is connected to the main grid through a transformer with a capacity of 20 p.u., equipped with an OLTC featuring 21 tap positions and covering a voltage range of $[0.9, 1.1]$ p.u.. Additionally, two capacitors with switching capability are installed at buses 53 and 64, each with a capacity of 0.4 p.u..

Two PV units are installed at buses 25 and 65. Each unit has a capacity of 2.6 p.u. and is connected to the network through an inverter with a capacity of 2.86 p.u. and a minimum admissible power factor of 0.9. This case study corresponds to a high penetration level of 100%, defined as the nominal total PV capacity divided by the peak load of the demands.

Two EV charging stations, ST1 and ST2, are installed at buses 15 and 60, respectively, each equipped with an ESS and a PV unit to supply EVs. Their technical and economic data are provided in Supplementary Material A Table SAI. The technical data of ESS and the cost of EV charging are obtained from [33] and [34], respectively.

To forecast the confidence bounds of uncertain data, appropriate autoregressive integrated moving average (ARIMA) models are fitted to historical data. Historical RT energy market prices are obtained from the PJM market [23], modeling the distribution system as part of the PJM market framework, with an energy hub assigned to each bus connected to the system. Historical irradiation data are obtained from the National Renewable Energy Laboratory [35] and converted into PV power generation. Additionally, historical data for EV charging active power levels are gathered from [36]. These data correspond to a fleet of 1000 EVs served by EV charging stations ST1 and ST2, which supply 20% and 80% of the fleet, respectively, with each EV traveling an average daily distance of 56.3 km.

An out-of-sample simulation is conducted to provide a more realistic assessment of the performance of the proposed model. The simulation is implemented in GAMS [37] using the CPLEX solver [38]. The confidence bounds of market prices are divided into intervals, enabling the determination of a price-power quantity pair for each interval, which is then used to submit a price-power curve for each hour. Once the actual realizations of uncertain data are known within each 15 min interval of the hour, the devices are dispatched. At this stage, no discrete variables are involved, and the operation problem becomes a second-order cone programming model, which is convex [28]. The optimal solution is thus guaranteed and can be efficiently obtained using commercial solvers such as CPLEX [38] and GUROBI [39].

B. Results

1) Impact of Uncertainty Budget

The performance of the proposed model is examined in detail for July 30, designated as the base day. Additionally, technical and economic metrics are compared across several other days. Two levels of uncertainty budget, $\Gamma^{\mathrm{RT}}=100\%$ and 30% of unknown market prices, are considered, corresponding to conservative and less conservative strategies, respectively. The conservative strategy safeguards decisions against all possible deviations, while the less conservative strategy reflects a practical approach in which the decision-maker accounts for some, but not all, deviations from the forecasted prices. Both strategies are consistent with real-world operational practices, where market participants balance protection against price uncertainty with the opportunity to capitalize on favorable price movements. These two risk attitudes have also been employed in previous studies on energy management [40] and volt-var control [41]. The uncertainty budgets Γ^{PV} and $\Gamma_s^{\mathrm{EV,C}}$ take the maximum value of 100% to protect constraints against related uncertainties. The penalty factor of voltage violations ω is set to be \$100.

Figures 1 and 2 illustrate the offering curves in the RT energy market at hours 8 and 13, respectively. It is observed that the willingness to sell energy at hour 13 is greater than that at hour 8. For instance, when $\Gamma^{\mathrm{RT}}=100\%$, the ADN decides to purchase energy at hour 8, submitting an offering curve within the power range $[1.07, 2.99]$p.u.. At hour 13, the willingness to purchase decreases while the willingness to sell increases relative to hour 8, resulting in an offering curve over the power interval $[-1.22, 1.42]$p.u.. This change occurs because the confidence bounds of the RT market price at hour 13 are higher than those at hour 8. In real energy markets, consistently elevated price expectations incentivize participants to shift toward selling positions and submit offers that capitalize on the broader upward price trend. The change in offering behavior between the two hours shown is driven primarily by anticipated price signals rather than fixed demand or generation schedules. This pattern aligns with how real-world participants increasingly rely on market forecasts and price-responsive strategies to enhance the profitability. Additionally, we observe that the risk strategy affects the offering curves. The small differences observed through two risk strategies suggest that, under the given market conditions, the impact of risk attitude on profitability is limited, though it may become more pronounced in markets with higher volatility or less predictable price patterns.

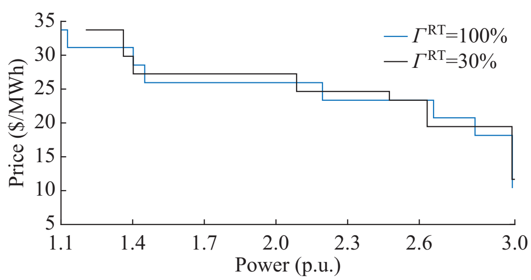

Fig. 1. Offering curve in RT energy market at hour 8.

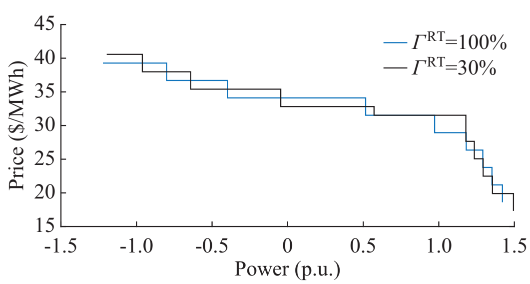

Fig. 2. Offering curve in RT energy market at hour 13.

Figure 3 shows the active power traded in the hourly RT energy market. The total power purchased in the RT energy market is equal to 45.9016 p.u. and 44.3564 p.u. for $\Gamma^{\mathrm{RT}}=$ 100% and 30%, respectively. By taking a less conservative strategy (i.e., $\Gamma^{\mathrm{RT}}=30\%$), the energy purchased from the RT energy market decreases by 3.36%.

In the fast timescale, the active power injected from/to the main grid may deviate from the scheduled active power settled in the RT energy market. Figure 4 depicts negative imbalances settled in the 15-min RT energy market during most sunny hours. This occurs because the ARO optimizes the energy traded in hourly RT energy market while protecting the problem against the worst case of uncertainty in the charging power level of EVs and the PV generation, i.e., their anticipated upper and lower bounds, respectively. As the actual charging power level of EVs is lower than its anticipated upper bound, and the actual PV generation is greater than its anticipated lower bound, the EMS and VVO units face a generation surplus, and therefore, negative energy imbalance occurs during most sunny hours. The PJM market exhibits two types of imbalances: positive and negative. A positive imbalance occurs when the ADN imports electricity from the main grid, whereas a negative imbalance occurs when surplus generation is exported back to the main grid. Accordingly, the ADN purchases and sells the positive and negative imbalances in the RT energy market, which can be represented as cost and revenue terms in the objective function, respectively.

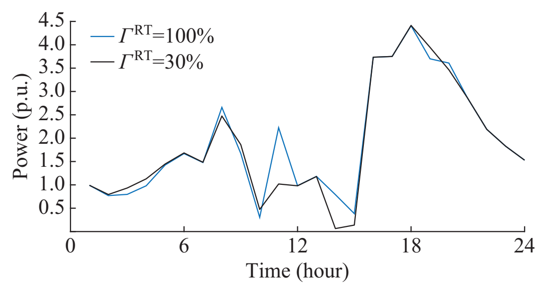

Fig. 3. Active power traded in hourly RT energy market.

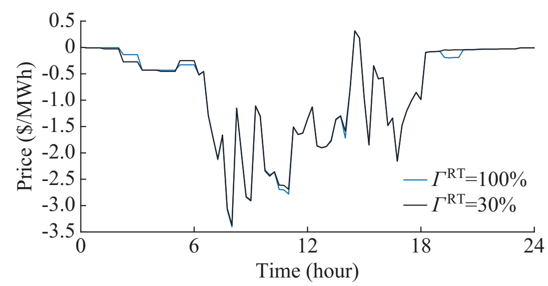

Fig. 4. Negative imbalance settled in 15-min RT energy market.

To gain a deeper understanding of the performance of the integrated EMS and VVO programs, an out-of-sample simulation is conducted over several days, from July 27 to July 30. The actual values of total profits, voltage violations, and energy losses are provided in Table II. It can be obtained from Table II that the percentage variations in profit and energy losses remain minor across different uncertainty budgets, which are below 0.5% and 1.5%, respectively, whereas voltage violations exhibit higher relative changes. This behavior aligns with the objective of maximizing profit and minimizing voltage violations. As voltage deviations are extremely small in magnitude, even slight absolute changes appear as large percentage variations. Furthermore, an inspection of the results indicates that when voltage violations are small, the impact of the uncertainty budget on the voltage profile across the buses is also negligible. Since energy losses depend primarily on voltage magnitude rather than on the voltage violation itself, small variations in voltage lead to correspondingly minor changes in energy losses.

TABLE II
ACTUAL VALUES OF TOTAL PROFITS, VOLTAGE VIOLATIONS, AND ENERGY LOSSES

Date	Total profit ($)		Voltage violation (10^{-5} p.u./h per bus)		Energy loss (p.u.)	
	Γ^{RT}= 100%	Γ^{RT}= 30%	Γ^{RT}= 100%	Γ^{RT}= 30%	Γ^{RT}= 100%	Γ^{RT}= 30%
July 27	2831.390	2833.317	0.0137	0.92	3.857	3.846
July 28	2967.335	2966.836	2.2000	2.47	5.704	5.726
July 29	3000.458	3000.106	2.9900	2.93	7.104	7.213
July 30	2947.052	2943.236	0.7470	1.44	5.224	5.255

2) *Sensitivity to Penalty Factor of Voltage Violations*

In order to investigate the impact of the penalty factor of voltage violations ω on the techno-economic metrics, we run the integrated EMS and VVO programs for the base day of July 30. ω takes different values of \$1, \$10, \$100, and \$1000.

Figure 5 shows the daily energy traded in the hourly RT energy market versus the daily value realized in the 15-min energy imbalance for different values of ω and Γ^{RT}. It is evident that the amount of the daily energy traded in the RT energy market decreases when ω changes from \$1 to \$1000 (3.74% and 2.97% decrease for $\Gamma^{RT}=100\%$ and 30%, respectively). In other words, by increasing ω, the ADN reduces the amount of energy it purchases from the hourly RT energy market. This is due to the fact that by choosing a higher ω, the offering curve moves left, and consequently, the ADN has a less/more willingness to buy/sell energy in the hourly RT energy market, as shown in Fig. 6. Meanwhile, as ω increases, the 15-min energy imbalance settled throughout the day decreases by 8.17% and 7.96% for $\Gamma^{RT}=100\%$ and 30%, respectively.

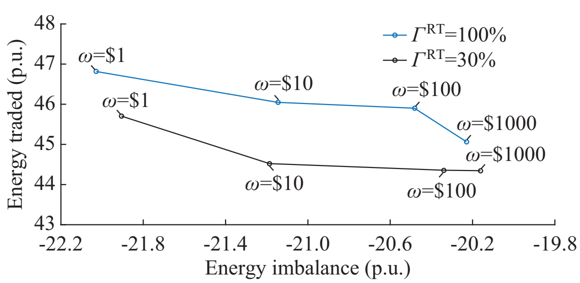

Fig. 5. Daily energy traded in hourly RT energy market versus daily value realized in 15-min energy imbalance for different values of ω and Γ^{RT}.

Figure 7 illustrates that by choosing a higher value of ω, both voltage violation and profit decrease. For $\omega=\$1$, the ADN experiences the highest voltage violation of 0.0188 and 0.0195 p.u./h per bus, as well as the highest profit of \$3047.167 and \$3044.312 under the uncertainty budgets of $\Gamma^{RT}=100\%$ and 30%, respectively. By raising the value of ω to \$1000, the voltage violation and the profit decrease by 99.99% and 3.48% for the two uncertainty budgets, respectively. The reduction in voltage violations accompanied by decreased profit stems from the effect of ω.

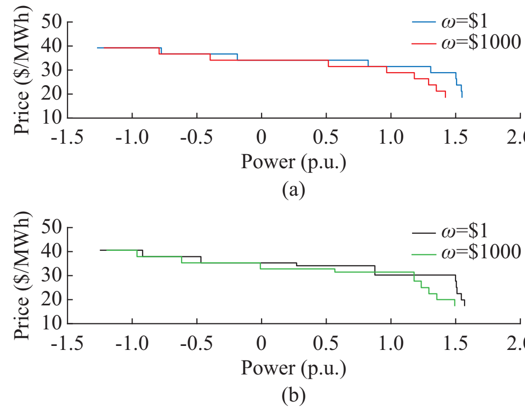

Fig 6. Offering curve in RT energy market at hour 13 for $\omega=\$1$ and \$1000. (a) $\Gamma^{RT}=100\%$. (b) $\Gamma^{RT}=30\%$.

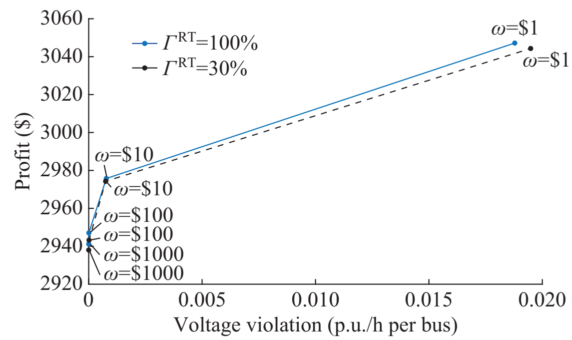

Fig. 7. Profit versus voltage violation for different values of ω.

Since voltage and load are positively correlated, higher voltages generally lead to greater energy consumption and higher demand utility. Most violations occur above the upper admissible voltage limit. Increasing ω lowers the voltage profile, mitigating these upper-limit violations but simultaneously reducing the demand utility, which, in turn, reduces the profit.

In Supplementary Material A, the deterministic optimization model (1)-(32) is run, and its performance is compared with that achieved by the proposed model.

VI. CONCLUSION

This paper proposes an ARO model for the operation of ADN in RT energy market, incorporating integrated EMS and VVO programs. The robustness level of the energy schedule is controlled by the uncertainty budget, while the extent of voltage violations across the distribution network is managed through a penalty factor in the objective function. Increasing the penalty factor results in smaller voltage deviations but reduces the actual profit, highlighting the trade-off between voltage regulation and economic performance. These results confirm that the proposed model effectively balances economic efficiency and voltage regulation.

Out-of-sample simulation conducted over several representative days demonstrates the robust performance of the proposed model. Profit and energy losses show negligible effects under varying uncertainty budgets of market prices, whereas voltage violations exhibit higher relative changes due to their small magnitudes. In addition, a 100% uncertainty budget is applied to PV power generation and EV charging power levels in the corresponding constraints to ensure the feasibility of scheduling decisions under all possible realizations of these uncertainties within their defined sets. Similar robustness evaluations based on extensive scenario-driven simulation have been reported in [13] and [27], where ARO is applied to MISOCP problems. These studies demonstrate that such formulations effectively maintain feasibility and stable operational performance under diverse uncertainty realizations, thereby supporting the robustness of the proposed model in this paper.

References

[1] M. Tahir, M. E. Nassar, R. El-Shatshat *et al.*, "A review of volt/var control techniques in passive and active power distribution networks," in *Proceedings of the 2016 4th IEEE International Conference on Smart Energy Grid Engineering*, Oshawa, Canada, Aug. 2016, pp. 57-63.

[2] S. Chowdhury, S. P. Chowdhury, and P. Crossley, *Microgrids and Active Distribution Networks*. London: The Institution of Engineering and Technology, 2009.

[3] M. Doostizadeh and H. Ghasemi, "Day-ahead scheduling of an active distribution network considering energy and reserve markets," *International Transactions on Electrical Energy Systems*, vol. 23, no. 7, pp. 930-945, Oct. 2013.

[4] P. Siano and D. Sarno, "Assessing the benefits of residential demand response in a real time distribution energy market," *Applied Energy*, vol. 161, pp. 533-551, Jan. 2016.

[5] A. Mohapatra, P. R. Bijwe, and B. K. Panigrahi, "An efficient hybrid approach for volt/var control in distribution systems," *IEEE Transactions on Power Delivery*, vol. 29, no. 4, pp. 1780-1788, Aug. 2014.

[6] R. Zafar, J. Ravishankar, J. E. Fletcher *et al.*, "Multi-timescale model predictive control of battery energy storage system using conic relaxation in smart distribution grids," *IEEE Transactions on Power Systems*, vol. 33, no. 6, pp. 7152-7161, Nov. 2018.

[7] Z. Wang, J. Wang, B. Chen *et al.*, "MPC-based voltage/var optimization for distribution circuits with distributed generators and exponential load models," *IEEE Transactions on Smart Grid*, vol. 5, no. 5, pp. 2412-2420, Sept. 2014.

[8] C. Sabillon-Antunez, O. D. Melgar-Dominguez, J. F. Franco *et al.*, "Volt-var control and energy storage device operation to improve the electric vehicle charging coordination in unbalanced distribution networks," *IEEE Transactions on Sustainable Energy*, vol. 8, no. 4, pp. 1560-1570, Oct. 2017.

[9] A. Zahedmanesh, K. M. Muttaqi, and D. Sutanto, "Active and reactive power control of PEV fast charging stations using a consecutive horizon based energy management process," *IEEE Transactions on Industrial Informatics*, vol. 17, no. 10, pp. 6742-6753, Oct. 2021.

[10] D. A. Quijano, A. Padilha-Feltrin, and J. P. S. Catalão, "Volt-var optimization with power management of plug-in electric vehicles for conservation voltage reduction in distribution systems," *IEEE Transactions on Industry Applications*, vol. 60, no. 1, pp. 1454-1462, Jan.-Feb. 2024.

[11] S. Najafi and H. Livani, "Robust day-ahead voltage support and building demand response scheduling under Gaussian mixture model uncertainty," *IEEE Transactions on Industry Applications*, vol. 61, no. 2, pp. 2352-2363, Mar.-Apr. 2026.

[12] S. Najafi and H. Livani, "Chance-constrained co-optimization of demand response and volt/var under Gaussian mixture model uncertainty," *Renewable Energy Focus*, vol. 53, p. 100674, Jun. 2025.

[13] H. Gao, J. Liu, and L. Wang, "Robust coordinated optimization of active and reactive power in active distribution systems," *IEEE Transactions on Power Systems*, vol. 33, no. 5, pp. 4436-4447, Sept. 2018.

[14] K. Christakou, M. Paolone, and A. Abur, "Voltage control in active distribution networks under uncertainty in the system model: a robust optimization approach," *IEEE Transactions on Smart Grid*, vol. 9, no. 6, pp. 5631-5642, Nov. 2018.

[15] X. Ke, N. Samaan, J. Holzer *et al.*, "Coordinative real-time sub-transmission volt-var control for reactive power regulation between transmission and distribution systems," *IET Generation, Transmission and Distribution*, vol. 13, no. 11, pp. 2006-2014, Nov. 2018.

[16] X. Zhu, J. Wang, N. Lu *et al.*, "A hierarchical VLSM-based demand response strategy for coordinative voltage control between transmission and distribution systems," *IEEE Transactions on Smart Grid*, vol. 10, no. 5, pp. 4838-4847, Sept. 2019.

[17] A. Dutta, S. Ganguly, and C. Kumar, "MPC-based coordinated voltage control in active distribution networks incorporating CVR and DR," *IEEE Transactions on Industry Applications*, vol. 58, no. 4, pp. 4309-4318, Jul.-Aug. 2022.

[18] M. S. Hossan and B. Chowdhury, "Integrated CVR and demand response framework for advanced distribution management systems," *IEEE Transactions on Sustainable Energy*, vol. 11, no. 1, pp. 534-544, Jan. 2020.

[19] K. Gholami, A. Azizivahed, A. Arefi *et al.*, "Risk-averse volt-var management scheme to coordinate distributed energy resources with demand response program," *International Journal of Electrical Power & Energy Systems*, vol. 146, p. 108761, Mar. 2023.

[20] E. Bektaş, K. Ç. Bayındır, A. Terciyanlı *et al.*, "Energy management integrated volt var optimization for distribution systems with SVR, PV inverter, and BESS: a case study in distribution system of Elazığ/Turkey," *Electrical Engineering*, vol. 105, no. 2, pp. 663-680, Apr. 2023.

[21] M. Azarnia, M. Rahimiyan, and P. Siano, "Offering of active distribution network in real-time energy market by integrated energy management system and volt-var optimization," *Applied Energy*, vol. 358, p. 122635, Mar. 2024.

[22] H. Kikusato, R. Ando, J. Hashimoto *et al.*, "Optimal short-term charge/discharge operation for electric vehicles with volt-var control in day-ahead electricity market," *IEEE Open Access Journal of Power and Energy*, vol. 11, pp. 410-420, Aug. 2024.

[23] PJM. (2025, Dec.). PJM interconnection. [Online]. Available: https://www.pjm.com/

[24] F. U. Nazir, B. C. Pal, and R. A. Jabr, "Approximate load models for conic OPF solvers," *IEEE Transactions on Power Systems*, vol. 36, no. 1, pp. 549-552, Jan. 2021.

[25] W. Gan, M. Shahidehpour, J. Guo *et al.*, "A tri-level planning approach to resilient expansion and hardening of coupled power distribution and transportation systems," *IEEE Transactions on Power Systems*, vol. 37, no. 2, pp. 1495-1507, Mar. 2022.

[26] D. Bertsimas and M. Sim, "The price of robustness," *Operations Research*, vol. 52, no. 1, pp. 35-53, Feb. 2004.

[27] T. Ding, C. Li, Y. Yang *et al.*, "A two-stage robust optimization for centralized-optimal dispatch of photovoltaic inverters in active distribution networks," *IEEE Transactions on Sustainable Energy*, vol. 8, no. 2, pp. 744-754, Apr. 2017.

[28] X. Cao, J. Wang, and B. Zeng, "A study on the strong duality of second-order conic relaxation of AC optimal power flow in radial networks," *IEEE Transactions on Power Systems*, vol. 37, no. 1, pp. 443-455, Jan. 2022.

[29] L. Baringo and M. Rahimiyan, *Virtual Power Plants and Electricity Markets: Decision Making Under Uncertainty*. Cham: Springer, 2020.

[30] H. Ahmadi, J. R. Martí, and H. W. Dommel, "A framework for volt-var optimization in distribution systems," *IEEE Transactions on Smart Grid*, vol. 6, no. 3, pp. 1473-1483, May 2015.

[31] National Renewable Energy Laboratory (NREL). (2021). End-use load profiles for the U.S. building stock. [Online]. Available: https://data.openei.org/submissions/4520

[32] J. R. Martí, H. Ahmadi, and L. Bashualdo, "Linear power-flow formulation based on a voltage-dependent load model," *IEEE Transactions on Power Delivery*, vol. 28, no. 3, pp. 1682-1690, Jul. 2013.

[33] World Energy Council. (2025, Dec.). Data of World Energy Council. [Online]. Available: https://www.worldenergy.org/

[34] Qmerit. (2025, Dec.). Data of Qmerit. [Online]. Available: https://qmerit.com/

[35] C. Maxey and A. Andreas, "Rotating Shadowband Radiometer (RSR): Oak Ridge, Tennessee (Data)," National Renewable Energy Laboratory, Tech. Rep. No. DA-5500-56512, 2007.

[36] U.S. Department of Energy. (2025, Dec.). Electric vehicle infrastructure projection tool (EVI-Pro) lite. [Online]. Available: https://afdc.energy.gov/evi-pro-lite

[37] GAMS Development Corporation. (2025, Dec.). GAMS. [Online]. Available: https://www.gams.com/

[38] IBM. (2025, Dec.). ILOG CPLEX. [Online]. Available: https://www.ibm.com/products/ilog-cplex-optimization-studio

[39] Gurobi Optimization, LLC. (2025, Dec.). Gurobi optimizer. [Online]. Available: https://www.gurobi.com/

[40] M. Rahimiyan and L. Baringo, "Strategic bidding for a virtual power plant in the day-ahead and real-time markets: a price-taker robust optimization approach," *IEEE Transactions on Power Systems*, vol. 31, no. 4, pp. 2676-2687, Jul. 2016.

[41] M. Azarnia and M. Rahimiyan, "Robust volt-var control of a smart distribution system under uncertain voltage-dependent load and renewable production," *International Journal of Electrical Power & Energy Systems*, vol. 134, p. 107383, Jan. 2022.

Ali Arab-Kuhsar received the B.Sc. and M.Sc. degrees from Bojnord University, Bojnord, Iran, and Shahrood University of Technology, Shahrood, Iran, in 2017 and 2023, respectively, both in electrical engineering. His research interests include distribution system operation, volt-var control and optimization, and electric vehicle.

Morteza Rahimiyan received the B.Sc. degree from Isfahan University of Technology, Isfahan, Iran, in 2003, and the M.Sc. and Ph.D. degrees (with honors) from Ferdowsi University of Mashhad, Mashhad, Iran, in 2006 and 2011, respectively, all in electrical engineering. He is currently an Associate Professor of Power and Energy Systems and Director of Energy Systems Planning and Operation Lab., Faculty of Electrical Engineering, Shahrood University of Technology, Shahrood, Iran. His research interests include planning and operation of power and energy system.

Pierluigi Siano received the M.Sc. degree in electronic engineering and the Ph.D. degree in information and electrical engineering from the University of Salerno, Salerno, Italy, in 2001 and 2006, respectively. He is a Full Professor of Electrical Power Systems and Scientific Director of the Smart Grids and Smart Cities Laboratory with the Department of Management & Innovation Systems, University of Salerno. His research interests include demand response, energy management, integration of distributed energy resources into smart grid, electricity market, and planning and management of power system.

Mahsa Azarnia received the B.Sc. degree in electric power engineering from Azarbaijan Shahid Madani University, Tabriz, Iran, in 2014, and the M.Sc. degree in power systems engineering from Shahrood University of Technology, Shahrood, Iran, in 2019. She is currently pursuing the Ph.D. degree with the Division of Energy Science, Luleå University of Technology, Skellefteå, Sweden. Her research interests include hosting capacity assessment, power system optimization, and volt-var control.